Preparation and Properties of Transparent Zinc Oxide/Silicone Nanocomposites for the Packaging of High-Power Light-Emitting Diodes

Yuping Sun, Aijuan Gu, Guozheng Liang, Li Yuan

Department of Materials Science and Engineering, College of Chemistry, Chemical Engineering and Materials Science, Soochow University, Suzhou 215123, China

ABSTRACT: New transparent zinc oxide (ZnO)/silicone nanocomposites with outstanding integrated properties, including a high UV-shielding efficiency and transparency, bigger thermal conductivity, and lower dielectric constant, were successfully developed; they were prepared by the uniform dispersion of organic modified nano-ZnO in a silicone matrix through *in situ* polymerization. The ZnO precursor was prepared by a direct precipitation method, which was then calcinated at different temperatures to produce nano-ZnO with various morphologies and sizes. The effects of the size, surface nature, and content of nano-ZnO on the key properties (e.g., optical and dielectric properties, thermal conductivities) of the composites were systematically investigated. The results show that the organic nano-ZnO prepared by 3-methacryloxypropyltrimethoxysilane can increase the dispersion of nano-ZnO in silicone resin, and the interfacial adhesion between inorganic and organic phases, and consequently improve the integrated properties of nanocomposites. The increase of the particle content and size of ZnO in composites can lead to high thermal conductivity and UV-shielding efficiency but lower visible-light transparency, so there is an optimum content and size of ZnO in composites to obtain the best integrated properties of the composites. Specifically, the nanocomposite containing 0.03 wt % organic nano-ZnO with an average size of 46 ± 0.4 nm not only had a high visible-light transparency, UV-shielding efficiency, and thermal conductivity but also possessed a low dielectric constant and loss and met the requirements of high-performance electronic packaging for high-power light-emitting diodes. © 2011 Wiley Periodicals, Inc. J Appl Polym Sci 121: 2018–2028, 2011

Key words: composites; dielectric properties; thermosets; transparency

INTRODUCTION

High-power light-emitting diodes (LEDs) have attracted great attention from scientists and engineers worldwide in recent years because of their many desirable advantages, including their long lifespan, low energy consumption, small size, high efficiency, and environmentally friendly characteristics.[1–5]

Packaging technology is one key and a necessary step for the practical application of LED lighting. Compared with traditional packaging materials for common LEDs, those for high-power LEDs should possess better integrated properties, especially UV resistance, thermal resistance, and transmittance.

This is because high-power LEDs, especially the white LEDs excited by a UV ray or a near-UV ray, have a higher luminescence intensity but also produce more heat and stronger short-wavelength radiation; this means that the lifetime of a high-power LED tends to be easily shortened by UV and heat radiation, not only from the environment but also from the LED itself.[6–11] Therefore, the packaging material for high-power white LEDs should possess a high UV-light-shielding efficiency to prevent the leakage of UV light and should maintain a high visible-light transparency, high thermal conductivity, and UV-irradiation resistance.

Silicone resins show great potential for high-power LED packaging because of their outstanding integrated properties, including their very low ionic impurities and moisture absorption, wide range of service temperatures, and stable thermooptical properties;[12–14] however, their thermal conductivity and UV irradiation resistance need to be improved to completely meet the requirements of high-power LEDs.

The development of organic–inorganic hybrids has been a vital subject because they have benefits for merging the advantages of both inorganic and

organic materials. To date, some inorganic filler/silicone hybrids have been prepared, including diamond/silicone and TiO_2/silicone,[15–18] and their results have proven that these hybrids have better thermal and mechanical properties than silicone resin. However, there has been no report on the preparation of UV-light-resistant transparent inorganic filler/silicone composites as packaging materials for high-power white LEDs.

Nano zinc oxide (ZnO) is an inorganic filler with an extremely high UV-shielding efficiency, low refractive index, and stable thermooptical properties; it shows big potential for the preparation of transparent high-UV-shielding efficiency composites.[19–21] For example, nano-ZnO/epoxy composites were prepared[22] and were proven to have an outstanding UV resistance and good processing characteristics. However, the transmittance of the nano-ZnO/epoxy composites significantly decreased in the wavelength range 400–450 nm, even for composites with an extremely low content (0.03 wt %) of nano-ZnO because of the poor dispersion of ZnO in the matrix; in addition, the thermal stability was not good enough to meet the harsh requirements of high-power LEDs because of the poor thermal resistance of epoxy resins.

The aim of this study was to develop a new kind of transparent nanocomposite with outstanding integrated properties, including a high UV-shielding efficiency, transparency, bigger thermal conductivity, and lower dielectric constant. Therefore, ZnO/silicone nanocomposites with various sizes, surface natures, and contents of nano-ZnO were prepared first; this was followed by a systematic investigation of the effects of the size, surface nature, and content of nano-ZnO on the key properties (e.g., optical and dielectric properties, thermal conductivities) of the ZnO/silicone nanocomposites. We expected to propose a new method for the development of high-performance packaging materials for high-power LEDs.

EXPERIMENTAL

Raw materials

A two-component transparent silicone resin (SP-3010A and SP-3010B) was purchased from Shenzhen Chunchang Silicone Rubber Co., Ltd. (Shenzhen, China). It crosslinked according to the mechanism of the hydrosilylation reaction, in which $-CH=CH_2$ and $Si-H$ react with each other. The A constituent was used as the silicone matrix, and the B component was used as the curing agent. 3-Methacryloxy-propyltrimethoxysilane (KH570) was bought from Shanghai Guipu Chemical Reagent, Ltd. (Shanghai, China). $Zn(NO_3)_2 \cdot 6H_2O$ (AR) and Na_2CO_3 (AR) were

commercial products and were not purified further before use. Distilled water was made in our laboratory.

Preparation of the ZnO nanoparticles

ZnO nanoparticles were prepared by a precipitation method.[22] First, 0.1 mol of $Zn(NO_3)_2 \cdot 6H_2O$ was dissolved in 0.2 mL of distilled water to form solution A, which was used as the stuff. Second, 0.12 mol of Na_2CO_3 was dissolved in 0.24 mL of distilled water to form solution B, which was used as the precipitant. Third, solution A was added dropwise to solution B with vigorous stirring, and then, white precipitates were derived from centrifugal precipitation; this was followed by washing with distilled water and ethanol. After that, the precipitates (which were the precursors of ZnO) were dried at 100°C for 6 h in a vacuum oven. Finally, the solids were calcinated at 300, 350, 400, 450, 500, and 600°C for 2 h, respectively, to obtain nano-ZnO particles with different sizes; they were denoted as Z1, Z2, Z3, Z4, Z5, and Z6, respectively.

Surface treatment of the ZnO nanoparticles

Two grams of Z1, 50 mL of methanol, and appropriate amount of KH570 were added to a flask; then, the flask was heated to 60°C and maintained at that temperature for 1 h under vigorous stirring. After that, particles were collected by centrifugal precipitation and washed with acetone three times; this was followed by drying *in vacuo* at 80°C for 12 h. The resultant product was coded as Z1(K).

Other surface-treated ZnO particles were also prepared according to the previous procedure, except that Z1 was replaced by Z2, Z3, Z4, Z5, or Z6, respectively, and the resulting particles were named Z2(K), Z3(K), Z4(K), Z5(K), and Z6(K), respectively.

Preparation of the ZnO/silicone nanocomposites

Z1(K) was blended with SP-3010B (the curing agent) at 25°C for 40 min with an ultrasonic technique, and then, SP-3010A (silicone resin) was added to the blend with stirring in an ice bath until a homogeneous mixture was obtained. The mixture was poured into a mold, followed by curing at 25°C for 24 h in a vacuum oven. The resulting composite was designed as Z1(K)-*n*/silicone, where *n* is the weight loading of Z1(K) per hundred weight of the composite.

Other nanocomposites were also prepared by the previously described procedure, except that Z1(K) was replaced by Z2(K), Z3(K), Z4(K), Z5(K), or Z6(K), respectively, and the resulting composites were designed as Z2(K)-*n*/silicone, Z3(K)-*n*/silicone,
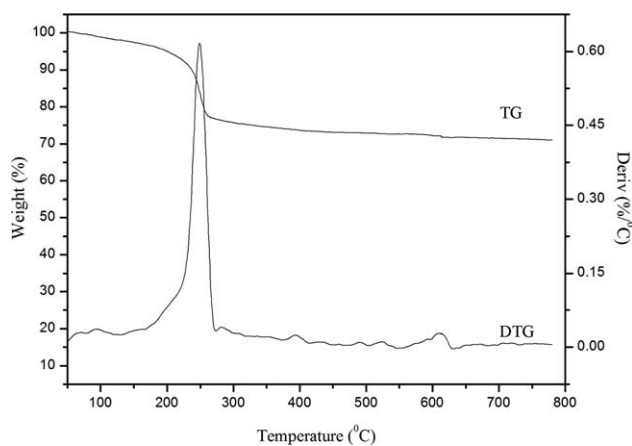
Figure 1 TG and derivative TG curves of the precursor for synthesizing ZnO.

Z4(K)-*n*/silicone, Z5(K)-*n*/silicone, and Z6(K)-*n*/silicone, respectively, where *n* represents the weight loading of ZnO in the composite.

Measurements

X-ray diffraction (XRD) spectra were recorded on a Bruker D8 ADVANCE diffractometer (Karlsruhe, Germany) with Cu Kα radiation ($\lambda = 0.15406$ nm) in the 15–75° (2θ) scanning range.

Thermogravimetric (TG) analysis was performed with PerkinElmer TGA-7 (Waltham, Massachusetts, USA) at a heating rate of 10°C/min in a nitrogen atmosphere from 50 to 800°C. The initial decomposition temperature was defined as the temperature at which the weight loss was 5%.

A laser particle analyzer system (Malvern HPP 5001, Malvern, Worcestershire, United Kingdom) was used to determine the mean particle size and distribution of nano-ZnO.

Fourier transform infrared (FTIR) spectra were recorded between 400 and 4000 cm^{-1} with a resolution of 2 cm^{-1} on a Nicolet 5700 infrared spectrometer (Madison, Wisconsin, the United States).

A scanning electron microscope (Hitachi S-4700, Tokyo, Japan) was used to observe the micromorphology of the fractured surfaces of the samples.

The optical properties were studied with an ultraviolet–visible (UV–vis) spectrophotometer (model Lambda 900, Waltham, Massachusetts, USA). The absorbance and transmittance spectra were scanned in the range 290–800 nm with a 2-nm interval.

The dielectric properties were tested with a broadband dielectric spectrometer (Novocontrol Concept 80 analyzer, Frankfurt, Germany) at 23 ± 2°C over a frequency range from 10 to 10^6 Hz.

The thermal conductivities at room temperature were characterized with a thermal constant analysis instrument (DRP-II, Xiangtan Instrument and Meter Factory, Xiangtan, China). Three samples with

dimensions of $(40 \pm 0.02) \times (40 \pm 0.02) \times (4 \pm 0.02)$ mm^3 were tested for each resin or composite to calculate the average value.

RESULTS AND DISCUSSION

Synthesis and characterization of the ZnO nanoparticles

There have been many reports about the preparation of nano-ZnO via a precipitation method; however, with regard to the same precursor, the size and its distribution of ZnO are greatly dependent on the calcination temperature.[23–26] Therefore, the properties of both the precursor and nano-ZnO need to be characterized herein.

The precursor for the preparation of ZnO was white spherical powder; its TG and derivative TG curves are depicted in Figure 1. The most significant weight loss occurred in the temperature range 190–260°C, and the maximum degradation temperature appeared at about 250°C; this was attributed to the removal of absorbed water and the decomposition of residual organic molecules. With increasing temperature, only a small amount of weight loss took place (specifically, the total loss weight was only about 28 wt % at 800°C), so 300°C was set as the initial calcination temperature in this study.

Figure 2 displays the XRD patterns of various ZnO nanoparticles obtained by the calcination procedure in air at different temperatures. The characteristic diffraction peaks of each sample were consistent with the standard (International Center for Diffraction Data, JCPDS 36–1451) and, thus, could be indexed to a pure hexagonal ZnO structure. In addition to the appearance of sharp diffraction peaks, no peaks assigned to other phases of ZnO or impurities were observed in Figure 2; this suggested that the
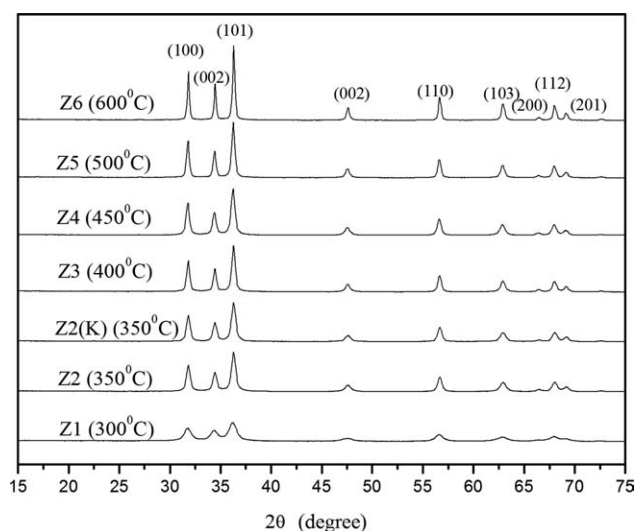

Figure 2 XRD patterns of various ZnO nanoparticles.

TABLE I
Mean Sizes of the ZnO Nanoparticles Estimated by the XRD Technique and Scherrer's Equation

Sample	Mean size (nm)
Z1	30 ± 0.4
Z2	46 ± 0.4
Z3	69 ± 0.2
Z4	75 ± 0.3
Z5	89 ± 0.2
Z6	132 ± 0.3
Z1(K)	28 ± 0.2
Z2(K)	40 ± 0.3
Z3(K)	64 ± 0.3
Z4(K)	75 ± 0.2
Z5(K)	86 ± 0.4
Z6(K)	121 ± 0.2

ZnO particles synthesized in this study had good crystallinity and high purity.

On the other hand, the characteristic peaks of ZnO became more intensive and narrow with increasing calcination temperature. This suggested that an elevated calcination temperature was beneficial for accelerating the growth of the ZnO nanoparticles.

In addition, the XRD patterns of Z2(K) were nearly the same as that of Z2; this showed that the surface treatment by KH570 did not change the crystal structure of Z2.

The mean size of ZnO nanoparticles was estimated with the half-widths of the diffraction peaks and Scherrer's equation,[27] and the corresponding data are summarized in Table I. The size of ZnO
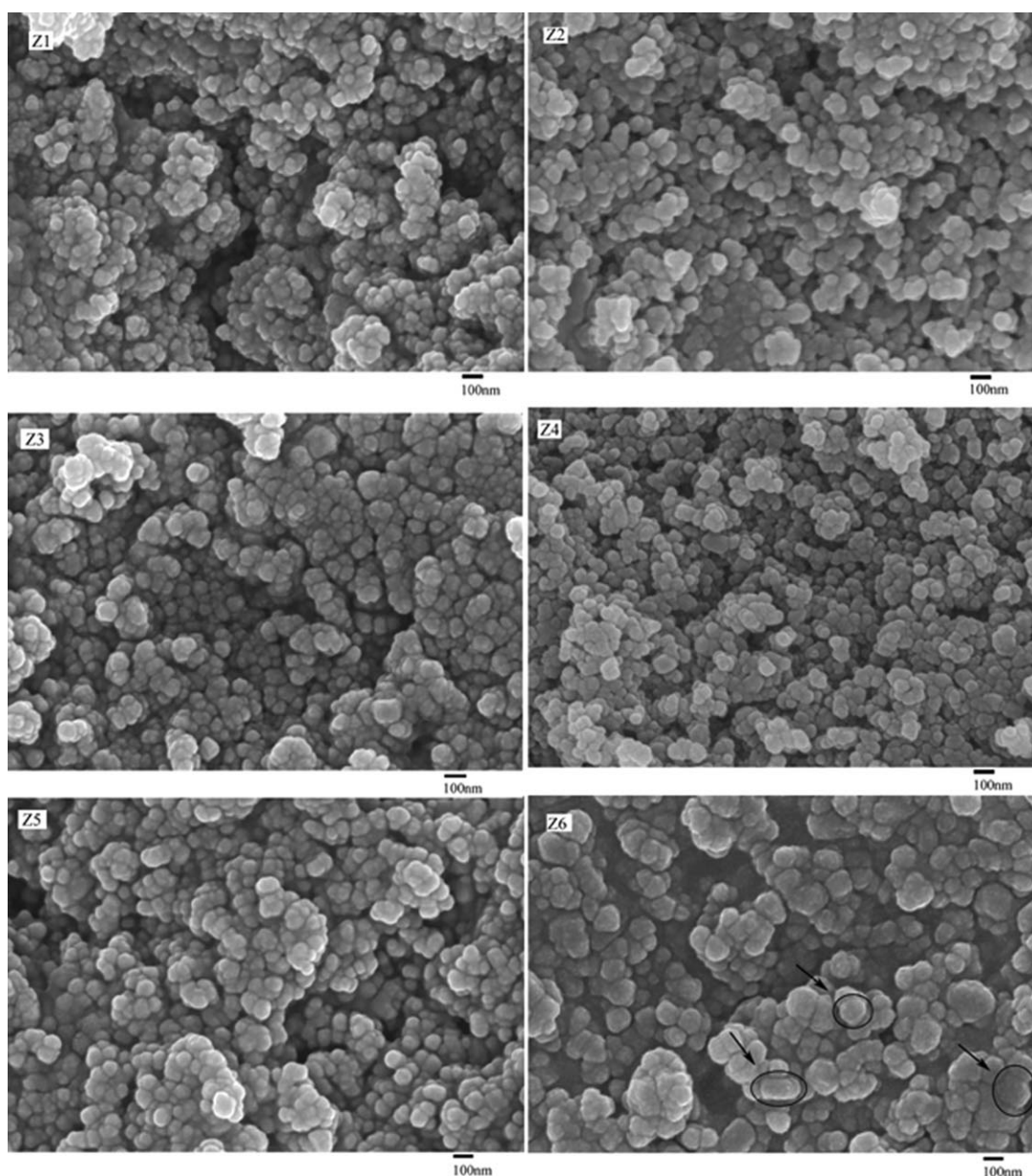

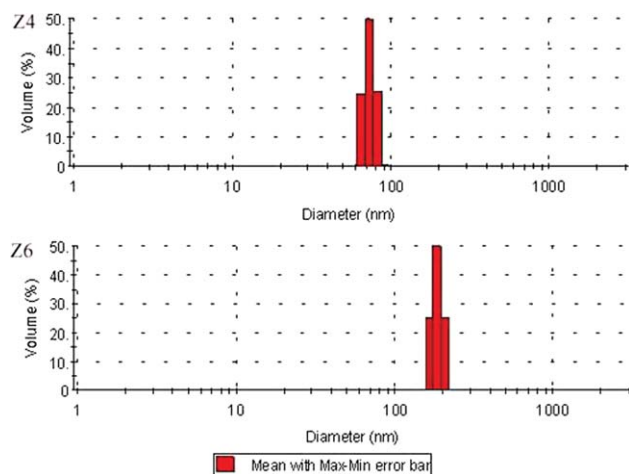**Figure 3** SEM micrographs of various ZnO nanoparticles.

Figure 4 Particle size distributions of Z4 and Z6. [Color figure can be viewed in the online issue, which is available at wileyonlinelibrary.com.]

was closely related to the calcination temperature. A high calcination temperature tended to produce ZnO with a large crystallite size, and this was further confirmed by the SEM images of various nano-ZnO particles, as shown in Figure 3.

As shown in Figure 3, nano-ZnO particles synthesized via the calcination at low temperature had a very fine size and a uniform spherical shape, whereas with increasing calcination temperature, the resulting ZnO particles showed a gradually increased dimension size. This was in good agreement with the data calculated by Scherrer's equation. Notably, when the calcination temperature was higher than 500°C, the morphology of the nano-ZnO particles changed from a homogeneous spherical shape to a mixed morphology consisting of short prismatics, hexagons, and quasi-sphericity. Further

increasing the calcination temperature, there were greater amounts of ZnO with nonuniform shapes. This phenomenon could be attributed to the polar growth and epitaxy in the growth of ZnO at high calcination temperatures.[28,29]

Because ZnO particles synthesized at calcination temperatures higher than 500°C had nonuniform shapes, the size and distribution of Z6 were determined by a laser particle size analyzer; similar analyses for Z4 were also done for comparison, and the corresponding curves are shown in Figure 4. There were 24.56, 49.56, and 25.44% of Z4 particles with sizes of 65.19, 73.21, and 82.21 nm, respectively; this was in good accordance with the apparent crystallite size determined by the XRD technique (Table I). However, there were 25.00, 50.00, and 25.00% of Z6 particles with sizes of 164.90, 185.20, and 208.00 nm, respectively, so the average size of Z6 particles was larger than that calculated by Scherrer's equation from XRD (Table I). The obvious difference between these data was attributed to the fact that Scherrer's equation was restricted to the small particles (usually smaller than 100 nm).[22] Figure 4 also shows that the size distribution of Z4 was narrower than that of Z6; this was also consistent with the result shown in Figure 3.

Effect of the size of ZnO on the optical properties of the ZnO/silicone nanocomposites

Figure 5 demonstrates the UV–vis transmittance and absorbance spectra of the silicone resin and various nanocomposites with different sizes. The silicone resin had a high visible-light transparency and UV-light transparency. In the case of the composites, their optical properties were closely dependent on the size of ZnO. In detail, Z1(K)-0.03/silicone exhibited a high and similar visible-light transparency as
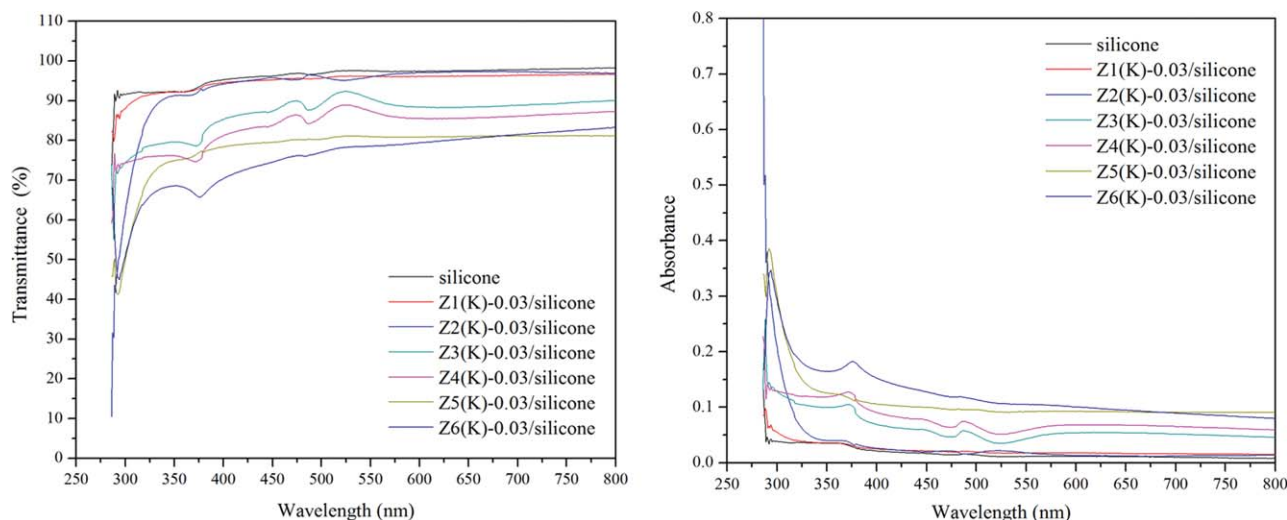

Figure 5 Overlay plots of the UV–vis transmittance and absorbance of the silicone resin and Z(K)-0.03/silicone nano-composites. [Color figure can be viewed in the online issue, which is available at wileyonlinelibrary.com.]
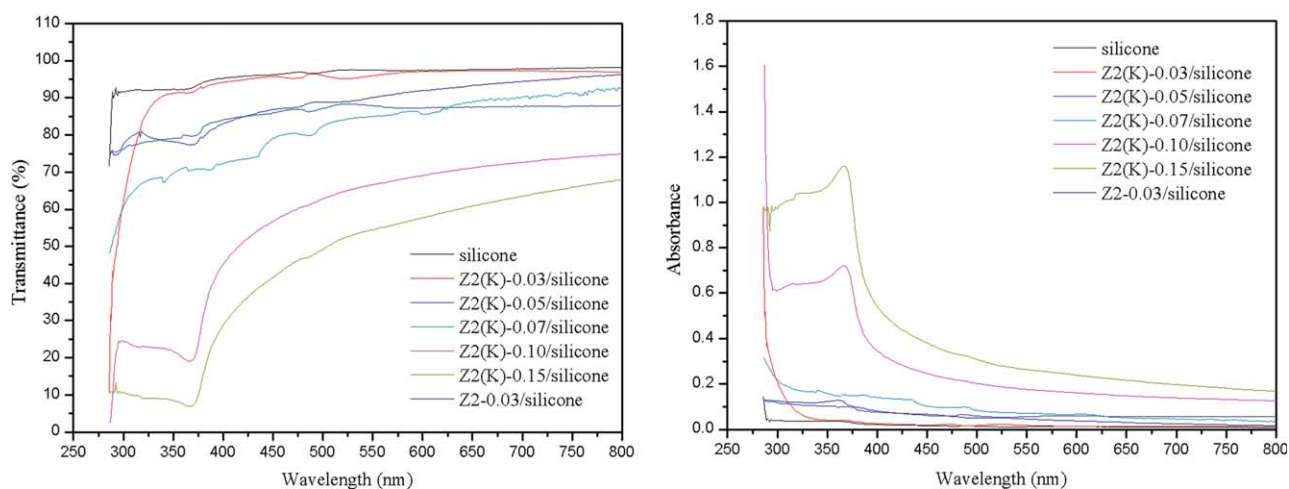
Figure 6 Overlay plots of the UV–vis transmittance and absorbance of the silicone resin and Z2-n/silicone nanocomposites. [Color figure can be viewed in the online issue, which is available at wileyonlinelibrary.com.]

the silicone resin, but the former did not have very high UV-light-shielding properties. However, the Z2(K)-0.03/silicone composite not only showed high UV-light shielding (ca. 60% at 300 nm and 20% at 370 nm), but it also exhibited a high visible-light transparency. These data were as good as that of the silicone resin, whereas other composites containing ZnO with larger sizes showed a decreased transmittance of UV light, especially in the wavelength range 300–380 nm. Specifically, the nanocomposites based on Z5 and Z6 showed a UV-shielding efficiency of 40% at 340 nm; this suggested that the nanocomposites based on nano-ZnO with larger sizes had good UV-shielding properties. In other words, their transparencies deteriorated.

The absorbance curve of the composite based on Z1 and Z2 almost overlaid that of the silicone resin, whereas the composite based on other particles showed a sharp absorption peak at 365 nm, of which the intensity increased with increasing size of ZnO in the composite. This was attributed to the blueshift phenomenon caused by the quantum size effect of the nano-ZnO particles. Because the blueshift was negative for the UV-shielding, it was important to choose a suitable size of nano-ZnO.

It is known that the UV-shielding capacity results from two contributions of ZnO, UV-light absorption and scattering,[30] which determine the intensity in the absorption peak. Nano-ZnO has an electronic structure of crystalline compounds, and there is a band gap around 3.3 eV (corresponding to 376 nm).[31] Because the light with a higher energy gap will be absorbed, all UV light with a length lower than 376 nm can be absorbed. On the other hand, light scattering will occur when light transmits through an inhomogeneous medium (e.g., composites) where the refractive index varies at different locations.[32] According to the light-scattering theory, there is a maximum value of light scattering when the filler particle size equals the half-wavelength of the incident light.[21] For UV light with a wave number between 300 and 380 nm, the maximum particle diameter of light scattering should be 150–190 nm; this was most similar to the size of Z6, so Z6 showed the highest UV-light scattering, and the UV-light transmittance decreased with increasing particle size.

Effect of the content of ZnO on the optical properties of the ZnO/silicone nanocomposites

Figure 6 shows the UV–vis transmittance and absorbance spectra of silicone resin and composites with various contents of Z2(K). Attractively, the Z2(K)-0.03/silicone composites had an almost similar outstanding visible-light transparency as the silicone resin. However, with increasing content of Z2(K), the transmittances of UV and visible lights of the composites generally decreased, and the UV absorbance increased. When the content of Z2(K) reached 0.15%, almost 90% UV radiation was shielded, but the transmittance of visible light was only 50%; this is not desirable for transparent packaging materials. Specifically, the composite with a loading of 0.03 wt % not only displayed good UV-shielding properties with a wide UV-wavelength range (ca. 60% at 300 nm and 20% at 370 nm) but also showed a high visible-light transmittance.

As discussed previously, the UV-shielding capacity results from UV-light absorption and scattering. It is known that a larger content of nano-ZnO tends to bring better UV-light absorption. Apart from that, the organic–inorganic interface of the nanocomposites also obviously increased with increasing particle content; this could have caused light scattering. The light scattering could have increased the UV-shielding capacity and reduced the transmittance of the nanocomposites, so the UV-light transmittance decreased with increasing content of nano-ZnO.
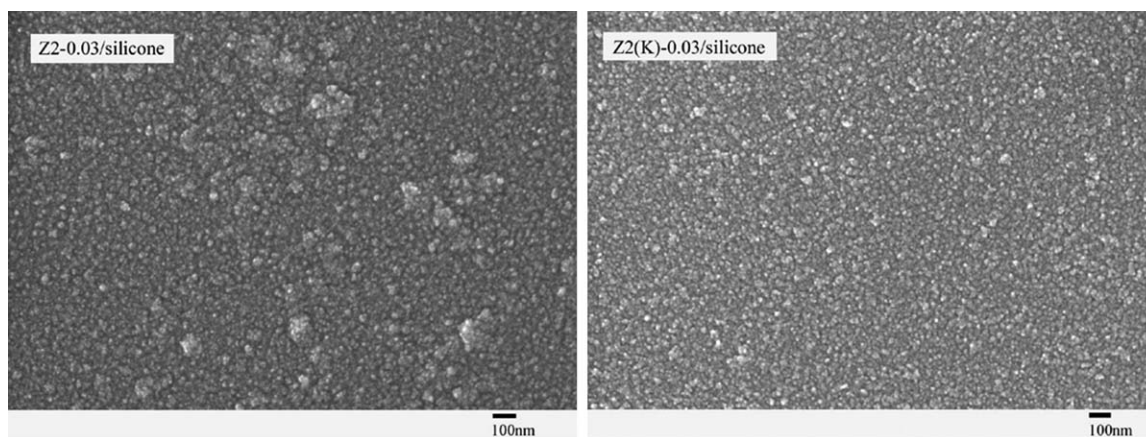
Figure 7 SEM micrographs of the Z2-0.03/silicone and Z2(K)-0.03/silicone composites.

Effect of the surface nature of ZnO on the optical properties of the ZnO/silicone nanocomposites

Figure 6 also displays the UV–vis transmittance and absorbance spectra of nanocomposites with different surface natures. The composite based on organic ZnO [Z2(K)] had almost the same spectra of both visible-light absorbance and transmittance as the silicone resin, but the composite based on original ZnO (Z2) showed increased absorbance and decreased transmittance; this suggested that the surface nature of ZnO also had an influence on the optical properties of composites.

To determine the reason behind the phenomenon, the morphologies of these composites were observed by the SEM technique, and corresponding pictures are shown in Figure 7. These two composites showed distinctly different morphologies; specifically, there were obvious agglomerations of Z2 in the silicone matrix, whereas Z2(K) particles were uniformly distributed throughout the polymer matrix. This resulted from the interaction between Z2(K) and silicone resin, as shown in Scheme 1.

The organic modification of ZnO took place according to a two-step mechanism. First, KH570 hydrolyzed to produce silanol (SiOH) groups, and second, silanol groups reacted with hydroxyl groups on the surface of ZnO.[33] This process could be proven by FTIR analyses. Figure 8 shows the FTIR spectra of Z2 and Z2(K); these two spectra were similar. Both of them had a strong absorption peak at 3440 cm^{-1}, attributed to the presence of —OH groups, whereas the intensities of these peaks decreased greatly after the organic modification of ZnO. Notably, compared with the spectrum of Z2, there were new peaks in the spectrum of Z2(K); they were the strong absorption at 830 cm^{-1}, reflecting Zn-O—Si groups,[34,35] and the absorption peaks in the region 2800–3000 cm^{-1}, assigned to the characteristic stretching vibration of —CH$_2$ and —CH$_3$ groups from KH570; this suggested that organic chains were successfully grafted on the surface of ZnO. On the other hand, the unsaturated double bonds on the organized ZnO could react with that of silicone resin. All these chemical bonds provided a guarantee for the good dispersion of ZnO in the silicone matrix, suitable interfacial adhesion, and good performance in the resulting composites.

Effects of the nature of ZnO on the dielectric properties of the ZnO/silicone nanocomposites

Figure 9(a) shows the variation of the dielectric constant with the frequency for silicone resin and composites based on nano-ZnO with different sizes. The measuring temperature was maintained constant during the whole testing process; hence, the influence of temperature on the dielectric behavior could not be considered. The silicone resin and all of the composites showed similarly excellent stable dielectric constants over the whole frequency range; interestingly, all of composites displayed an even slightly lower dielectric constant than the silicone resin. Because all of the composites showed a similar dielectric constant, we suggest that the size of the nano-ZnO did not play an important role in determination of the dielectric constant.

Figure 9(b) shows the dependence of the dielectric constant on the frequency of the Z2(k)-n/silicone nanocomposites with various contents of Z2(k). A small addition (e.g., <0.07%) of nano-ZnO into silicone resin decreased the dielectric constant from 2.87 to 2.76, whereas when the filler loading was larger than 0.07%, the dielectric constant of the nanocomposite was slightly higher than that of the silicone resin.

The dielectric loss was more frequency-dependent than the dielectric constant but concrete values seemed independent of the particle size and content of ZnO (Fig. 10). This is very attractive for practical applications.
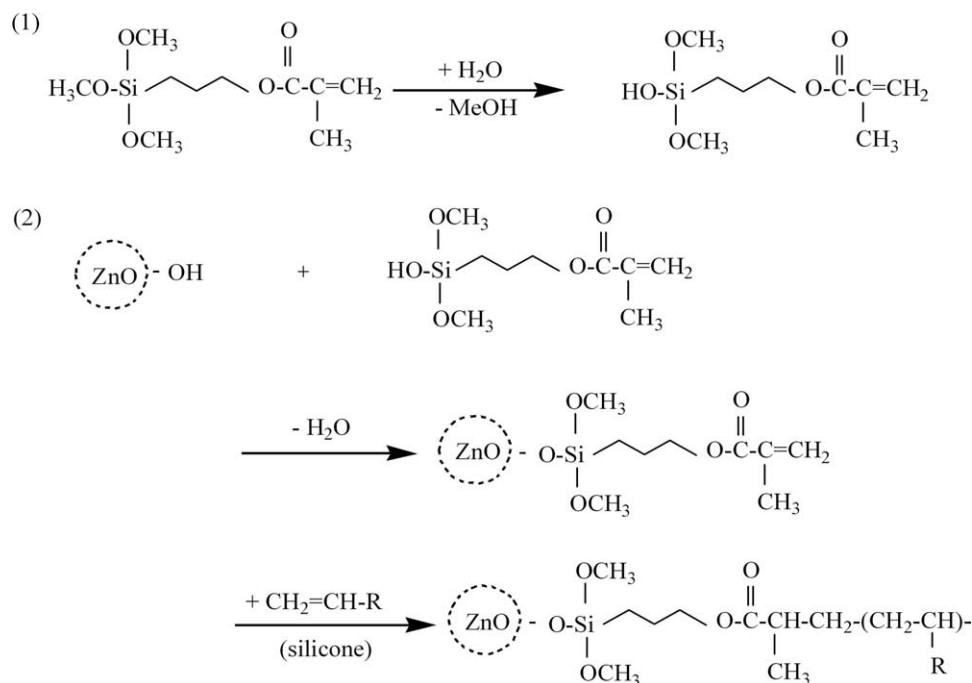
Scheme 1 Mechanism of the surface treatment of ZnO and the interaction between the treated ZnO with silicone resin.

It is known that the dielectric properties of a polymeric composite depend on the orientation and relaxation of dipoles in the applied electric field.[36] The process of dipole polarization is accompanied by the movement of polymer chain segments; therefore, the dielectric properties are closely related to the structure of the composite. Generally, inorganic fillers in a composite can restrict the mobility of molecular chains;[37] this role will be significantly enhanced when there is a chemical reaction between the fillers and the organic matrix and, thus, result in a decreased dielectric constant and loss. This statement was further confirmed by the data shown in Figures 9(b) and 10(b); that is, the dielectric constant and loss of Z2(K)-0.03/silicone were lower than that of the Z2-0.03/silicone composite over the whole frequency range. In the case of the prepared composites, the active groups on the surface of ZnO(K) reacted with the silicone resin, so the movement of molecules was restricted in the applied electric field and, thus, led to a decreased dielectric constant. However, with increasing content of ZnO(K), the interfacial effect could not be neglected; this resulted in an enlarged dielectric constant.

On the basis of the previous discussion, we can state that the content, size, and surface nature of ZnO had effects on the dielectric properties (especially the dielectric constant) of the composites, but the variety of dielectric properties was small; in other words, the composites developed herein had excellent dielectric properties compared to the silicone resin and showed great potential for electronic packaging.

Effects of the nature of ZnO on the thermal conductivities of the ZnO/silicone nanocomposites

Thermal dissipation is one key issue in electric packaging; a material with high thermal dissipation has been one hot topic for worldwide applications. It is known that the thermal conductivity of nano-ZnO is 25 W m^{-1} K^{-1};[38] this is much larger than that of the silicone resin (0.356 W m^{-1} K^{-1}). Therefore, it was not surprising to find that the ZnO(K)/silicone nanocomposites had bigger thermal conductivities than the silicone resin and that the larger the content
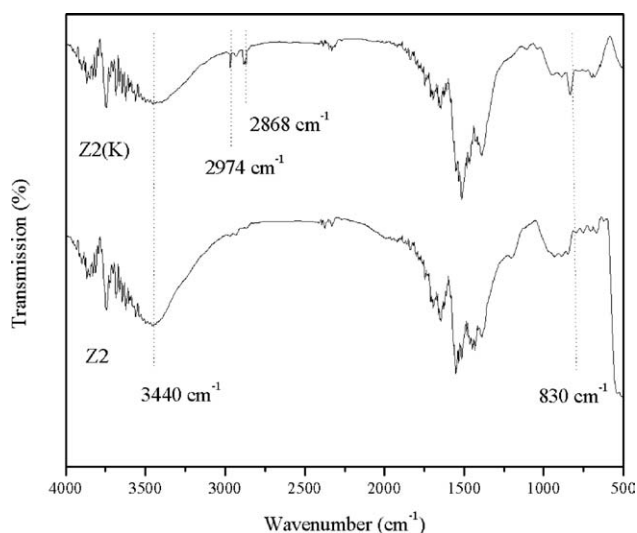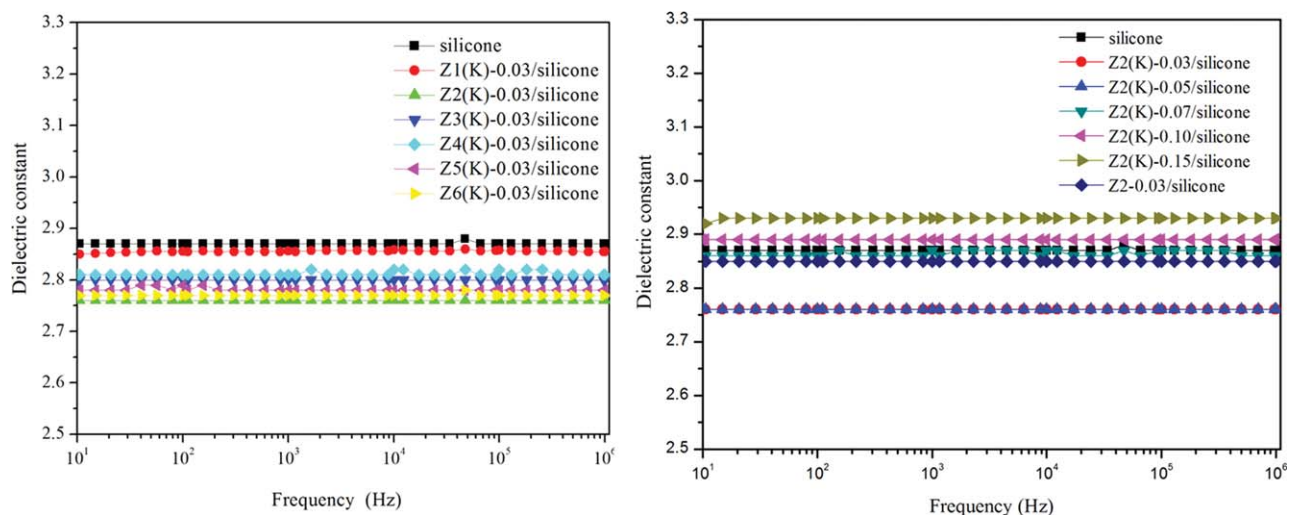

Figure 8 FTIR spectra of Z2 and Z2(K).

Figure 9 Dependence of the dielectric constant on the frequency of the silicone resin and various nanocomposites. [Color figure can be viewed in the online issue, which is available at wileyonlinelibrary.com.]

of ZnO was, the bigger the thermal conductivity was (Fig. 11). For example, when the content of Z2(K) was 0.15%, the thermal conductivity of the composite was 0.649 W m^{-1}K^{-1}; this was about 1.7 times of that of the silicone resin.

It was interesting to find that with the same content of ZnO, the composite based on a larger size of ZnO tended to have a bigger thermal conductivity (Fig. 12). This may have been due to the fact that the fillers with a larger size in the nanocomposites showed fewer contact points and a smaller contact area with the matrix; accordingly, the phonon scattering and interface thermal resistance in the heat-transfer process were relatively small.[39] Because the total thermal conductivity consisted of the phonon contribution and the carrier contri-

bution,[40] the composites based on ZnO with larger sizes tended to have bigger thermal conductivities.

Figure 11 also shows that the uniform dispersion of particles in the composites was beneficial for improving the thermal conductivity. It is known that surface treatment not only increases the dispersion of inorganic fillers in the organic matrix but also improves the compatibility between the inorganic and organic phases. The good dispersion of the particles can form a relatively good thermal path, and the good interface adhesion is helpful for reducing phonon scattering; this leads to improved thermal conductivities in the nanocomposites. Consequently, the thermal conductivities of Z2(K)-0.03/silicone were relatively bigger.
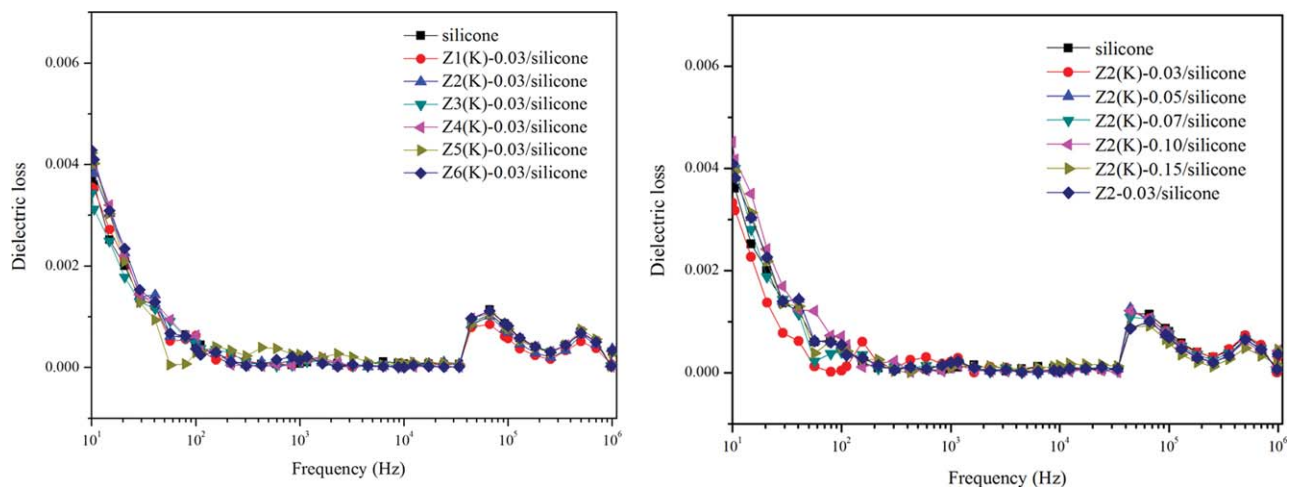

Figure 10 Dependence of the dielectric loss on the frequency of the silicone resin and various nanocomposites. [Color figure can be viewed in the online issue, which is available at wileyonlinelibrary.com.]
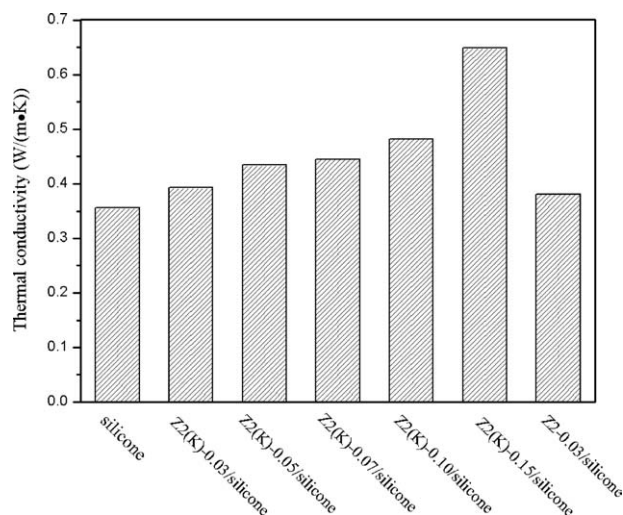
Figure 11 Thermal conductivities of the silicone resin and Z2/silicone nanocomposites.

CONCLUSIONS

New transparent ZnO/silicone nanocomposites with outstanding integrated properties, including a high UV-shielding efficiency and transparency, bigger thermal conductivity, and a lower dielectric constant, were successfully developed.

The integrated properties of the composites were closely related to the size, content, and surface nature of ZnO. The organic nano-ZnO prepared by 3-methacryloxypropyltrimethoxysilane increased not only the dispersion of nano-ZnO in the silicone resin but also the interfacial adhesion between the inorganic and organic phases and, thus, improved the integrated properties of the nanocomposites, which included high visible- and UV-light-shielding effi-
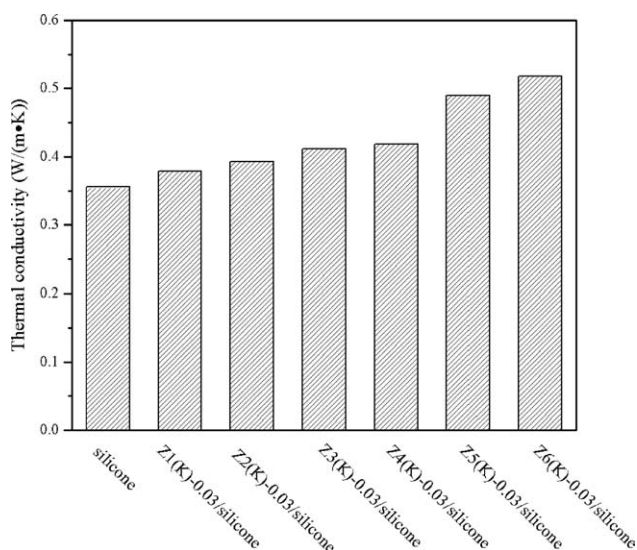
ciencies, large thermal conductivities, and a low dielectric constant.

The increase in the particle content and size of ZnO in the composites led to a higher thermal conductivity and UV-light-shielding efficiency but a lower visible-light transparency, so there was an optimum content and size of ZnO in the composites for obtaining the best integrated properties. Specifically, the nanocomposite containing 0.03 wt % nano-ZnO(K) with an average size of 46 ± 0.4 nm not only had a high visible-light transparency and UV-light-shielding efficiency and a large thermal conductivity but also possessed a low dielectric constant and loss; thus, it met the requirements of high-performance electronic packaging for high-power LEDs.

References

1. Kim, L.; Choi, J. H.; Jang, S. H.; Shin, M. W. Thermochim Acta 2007, 455, 21.
2. Lu, X. Y.; Hua, T. C.; Liu, M. J.; Cheng, Y. X. Thermochim Acta 2009, 493, 25.
3. Kim, J. K.; Schubert, E. F. Opt Express 2008, 16, 21835.
4. Moreno, I.; Bermúdez, D.; Avendaño-Alejo, M. Appl Optics 2010, 49, 12.
5. Craford, M. G. J Light Visual Environ 2008, 32, 58.
6. Norris, A. W.; Bahadur, M.; Yoshitake, M. Proc SPIE-Int Soc Opt Eng 2005, 5941, 207.
7. Huang, W.; Zhang, Y.; Yu, Y. Z.; Yuan, Y. X. J Appl Polym Sci 2007, 104, 3954.
8. Liu, S.; Yang, J. H.; Gan, Z. Y.; Luo, X. B. Int J Therm Sci 2008, 47, 1086.
9. Arik, M.; Setlur, A.; Weaver, S.; Haitko, D.; Petroski, J. J Electron Packaging 2007, 129, 328.
10. Li, Y. Q.; Yang, Y.; Fu, S. Y. Compos Sci Technol 2007, 67, 3465.
11. Christensen, A.; Graham, S. Appl Therm Eng 2009, 29, 364.
12. Yang, Y.; Li, W. N.; Luo, Y. S.; Xiao, H. M.; Fu, S. Y.; Mai, Y. W. Polymer 2010, 51, 2755.
13. Si, Q. F.; Fan, X. D.; Liu, Y. Y.; Kong, J.; Wang, S. J.; Qiao, W. Q. J Polym Sci Part A: Polym Chem 2006, 44, 3261.
14. Chevalier, P.; Ou, D. L.; Lee, Y.; Robson, S.; Dupont, A. Macromol Symp 2006, 233, 117.
15. Cao, M. L.; Pang, F. Y.; Zhang, M. C.; Cheng, Z. J.; Gao, Y.; He, P. G.; Pan, L. K.; Sun, Z. In 2nd IEEE International Nanoelectronics Conference; Inst. Of Elec. And Elec. Eng. Computer Society: Washington, DC, 2008; p 758.
16. Mu, Q. H.; Feng, S. Y.; Diao, G. Z. Polym Compos 2007, 28, 125.
17. Sim, L. C.; Ramanan, S. R.; Ismail, H.; Seetharamu, K. N.; Goh, T. J. Thermochim Acta 2005, 430, 155.
18. Han, Y.; Kiat-Amnuay, S.; Powers, J. M.; Zhao, Y. M. J Prosthet Dent 2008, 100, 465.
19. Li, H. Y.; Chen, Y. F.; Ruan, C. X.; Gao, W. M.; Xie, Y. S. Nanopart Res 2001, 3, 157.
20. Zhou, S. X.; Wu, L. M.; Xiong, M. N.; He, Q. Y.; Chen, G. D. J Dispersion Sci Technol 2005, 25, 417.
21. Xiong, M. N.; Gu, G. X.; Wu, L. M. J Appl Polym Sci 2003, 90, 1923.
22. Li, Y. Q.; Fu, S. Y.; Mai, Y. W. Polymer 2006, 47, 2127.
23. Kanade, K. G.; Kale, B. B.; Aiyer, R. C.; Das, B. K. Mater Res Bull 2006, 41, 590.
24. Chen, C. C.; Liu, P.; Lu, C. H. Chem Eng J 2008, 144, 509.
25. Zheng, R. K.; Liu, H.; Zhang, X. X.; Roy, V. A. L.; Djurišiæ, A. B. Appl Phys Lett 2004, 85, 2589.

Figure 12 Thermal conductivities of the silicone resin and Z(k)-0.03/silicone nanocomposites.

26. Dong, Z. M.; Fan, L. Z.; Zhao, S. J.; Nan, C. W. Mater Sci Eng B 2003, 99, 386.
27. Hong, R. Y.; Li, J. H.; Chen, L. L.; Liu, D. Q.; Li, H. Z.; Zheng, Y.; Ding, J. Powder Technol 2009, 189, 426.
28. Han, Y. X.; Ding, Y. Z.; Yin, W. Z.; Ma, Z. X. Trans Nonferrous Met Soc China 2006, 16, 1205.
29. Pardesi, S. K.; Patili, A. B. J Mol Catal A 2009, 308, 32.
30. Scierka, S.; Drzal, P. L.; Forster, A. L.; Svetlik, S. Mater Res Soc Symp Proc 2005, 841, 217.
31. Wood, A.; Giersig, M.; Hilgendorff, M.; Vilas-Campos, A.; Liz-Marzan, L. M.; Mulvaney, P. Aust J Chem 2003, 56, 1051.
32. Yang, H. Y.; Zhu, S. K.; Pan, N. J Appl Polym Sci 2004, 92, 3201.
33. Tang, E. J.; Cheng, G. C.; Pang, X. S.; Ma, X. L.; Xing, F. B. Colloid Polym Sci 2006, 284, 422.

34. Guo, Z. H.; Wei, S. Y.; Shedd, B.; Scaffaro, R.; Pereira, T.; Hahn, H. T. J Mater Chem 2007, 17, 806.
35. Ma, J. G.; Liu, Y. C.; Xu, C. S.; Liu, Y. X.; Shao, C. L.; Xu, H. Y.; Zhang, J. Y.; Lu, Y. M.; Shen, D. Z.; Fan, X. W. J Appl Phys 2005, 97, 103509.
36. Hong, J. I.; Winberg, P.; Schadler, L. S.; Siegel, R. W. Mater Lett 2005, 59, 473.
37. Singha, S.; Thomas, M. J. IEEE Trans Dielectr Electr Insul 2008, 15, 12.
38. Lakshmi, P. V. B.; Ramachandran, K. Int J Thermophys 2007, 28, 1353.
39. Du, F.; Guthy, C.; Kashiwagi, T.; Fischer, J. E.; Winey, K. I. J Polym Sci Pol Phys 2006, 44, 1513.
40. Zhao, X. B.; Ji, X. H.; Zhang, Y. H.; Zhu, T. J.; Tu, J. P.; Zhang, X. B. Appl Phys Lett 2005, 86, 062111–1.